Model for the dynamics of a water cluster in an x-ray free electron laser beam

Magnus Bergh, Nicuşor Tîmneanu, and David van der Spoel*
Department of Cell and Molecular Biology, Biomedical Centre, Box 596, Uppsala University, S-75124 Uppsala, Sweden
(Received 7 May 2004; published 11 November 2004)

A microscopic sample placed into a focused x-ray free electron laser beam will explode due to strong ionization on a femtosecond time scale. The dynamics of this Coulomb explosion has been modeled by Neutze *et al.* [Nature (London) **406**, 752 (2000)] for a protein, using computer simulations. The results suggest that by using ultrashort exposures, structural information may be collected before the sample is destroyed due to radiation damage. In this paper a method is presented to include the effect of screening by free electrons in the sample in a molecular dynamics simulation. The electrons are approximated by a classical gas, and the electron distribution is calculated iteratively from the Poisson-Boltzmann equation. Test simulations of water clusters reveal the details of the explosion dynamics, as well as the evolution of the free electron gas during the beam exposure. We find that inclusion of the electron gas in the model slows down the Coulomb explosion. The hydrogen atoms leave the sample faster than the oxygen atoms, leading to a double layer of positive ions. A considerable electron density is located between these two layers. The fact that the hydrogens are found to explode much faster than the oxygens means that the diffracting part of the sample stays intact somewhat longer than the sample as a whole.

DOI: 10.1103/PhysRevE.70.051904 PACS number(s): 82.53.Ps, 52.65.Yy

I. INTRODUCTION

The dawning of the x-ray free electron laser era has triggered new research in wide areas of science. The combination of high-intensity laser light and a pulse length in the femtosecond regime will provide a unique tool for probing matter [1–3]. It has been suggested [4,5] that the x-ray free electron laser (XFEL) could have the potential for imaging single biomolecules or small assemblies of biomolecules—e.g., a virus particle. In that case, the resolution of the structural information will be limited by the formation of radiation damage in the sample. The photoelectric effect, which is the main process in the interaction of x rays with organic molecules, leads to strong ionization of the sample, ultimately causing a Coulomb explosion. The dynamics of the explosion can, in principle, be modeled with computer simulations. This was done [5] using an extension of the GROMACS molecular dynamics package [6]. This paper deals with further improvements of this model, in order to include the effect of free electrons in the sample on explosion dynamics.

At 1 Å wavelength, the energy of the ejected photoelectrons is about 12 keV and the cross section for collision with atoms and ions is low [7]. These electrons will most likely escape a small sample in less than a femtosecond. Most ions are left with a *K*-shell vacancy, which leads to the emission of an Auger electron within a few femtoseconds for lighter elements. These electrons have a lower energy (250 eV and 508 eV for carbon and oxygen, respectively [8]) and may be caught in the sample, causing further ionizations through interaction with atoms and ions. The Coulomb interaction between ions, which drives the explosion, will be screened by the free electrons within the sample, as was recently shown in a hydrodynamic model [9]. That one-dimensional continuum model can simulate the hydrodynamic expansion of large biomolecules, but it assumes spherical symmetry of the sample. The electron screening is also described in another model, where the trajectory of each electron is followed classically [10].

In the calculations of Neutze *et al.* [5], the movement of the atoms was simulated by numerically solving Newton's equations of motion, which is the principle for molecular dynamics. Chemical bonds were described by Morse potentials [11], and nonbonded interactions were described by van der Waals (effective pair potentials) and Coulomb (pair additive) interactions. The interaction of the photon beam with the atoms in the sample was simulated stochastically. At each time step, each atom and ion had a certain probability for elastic, inelastic, photoelectric events, proportional to the respective cross sections, and Auger decays, proportional to the measured Auger decay rates [7]. Every ionization was kept track of, and cross sections were updated to account for electron depletion.

In the present work, the screening by free electrons is modeled by introducing an electron gas that adapts itself to the electrostatic environment created by all charges in the sample, at each time step of the simulation. It has been suggested [5] that the screening by free electrons would have a large impact on the dynamics of an exploding molecule in an XFEL beam, and an accurate simulation is important when it comes to planning experiments and designing experimental equipment. Due to the heavy ionization of the system, the long-range Coulomb interaction is the dominating mechanism for the explosion. This obviously implies that the dynamics of the system will be sensitive to the treatment of the Coulomb interactions. As a simulation of a protein will involve thousands of atoms and the computational cost of the pairwise Coulomb interactions scales as N^2, the particle mesh Ewald [12] (PME) method is used, which scales as $N \ln(N)$. A drawback of this method is that an artificial periodicity is imposed on the system, but the clear advantage is

*Electronic address: spoel@xray.bmc.uu.se

that it allows us to treat all charges in the sample efficiently and accurately.

II. THEORY

Free electrons can appear in the system through three processes: photoionization, Auger decay, or secondary ionization from moving electrons. The photoelectrons will have a small effect for large macromolecules or complexes [9], but are not considered at this stage. The Auger electrons have a lower probability of escaping the sample and are more likely to accumulate and interact with atoms and ions. The test simulation in this paper is based on the assumption that an Auger electron generates secondary electrons during the average time it takes to travel through the cluster [13], after which it escapes. The potential inside our studied sample is not high enough to capture the scattered Auger electrons, as is the case for larger samples [9,14]. As the elastic scattering of electrons on atoms and ions does not alter the electric charge or the energy of the system, this process is neglected in the direct simulation. The inelastic scattering, on the other hand, has the effect of reducing the electron temperature and causing further ionizations. This process is not properly understood, but approximate models for organic molecules are under development [13,15,16]. The rate of generated secondary electrons and their energy in water is based on simulations of the dynamics of the scattering of Auger electrons in ice and water [13], which includes a complete treatment of the elastic and inelastic scattering of the free electrons. The free electrons can also interact directly with the incoming photons through Compton scattering. We have estimated that the inelastic cross section for this process is about two orders of magnitude lower than the cross section for atomic scattering, and it can therefore be neglected at the present level of accuracy.

The free electrons in the sample are modeled as a classical electron gas. The validity of this assumption can be checked with the plasma approximation $\rho\lambda_D^3 \gg 1$ and $R \gg \lambda_D$, where ρ is the electron density, λ_D is the Debye length, and R is the radius of the sample. In this approximation, there should be a statistically significant number of electrons within a sphere with a radius equal to the Debye length, and the system should be larger than the Debye length. The plasma approximation is valid during most of the simulation. The first inequality will not be true in the very beginning of the pulse, due to the low number of free electrons. However, at an early stage the electron screening is negligible. At the end of the simulation, the second inequality might also break down because of the low electron temperature, giving a strongly coupled plasma, but at this late stage the sample is already destroyed by the Coulomb explosion. It is reasonable to assume an isotropic electron cloud [15,16], due to the fact that the gas will consist of Auger electrons and slower secondary electrons, spread out evenly in the sample. Since the electron-electron collisions have a time scale of ≈ 1 fs and the inelastic scattering of electrons is somewhat faster [13,16], the velocity distribution is not strictly Maxwellian. The cross section for inelastically scattered electrons in water has a peak around 100 eV and drops drastically for energies below 10 eV [13]. Thus, when the number of secondary electrons starts to increase and the screening will take effect, the electron energy distribution will have a maximum and descend toward zero for lower energies, as well as decreasing for higher energies. This qualitative estimate motivates the use of a simple Maxwell-Boltzmann distribution for the electrons, using an average electron temperature.

The electrostatic potential ϕ in a system containing free electrons can be described by the Poisson equation

$$\Delta\phi(x,y,z) = -\rho(x,y,z)/\epsilon_0, \tag{1}$$

where $\rho(x,y,z)$ is the total charge distribution of bound (possibly fractional) and free charges. The potential energy of each electron will be $-e\phi(x,y,z)$, where e is the electron charge. Hence, assuming the Maxwell-Boltzmann statistics to be a valid approximation, the electron density will change from an initial value ρ_{e0} in a neutral environment to

$$\rho_e(x,y,z) = \rho_{e0} \exp[e\phi(x,y,z)/k_B T], \tag{2}$$

where T is the electron temperature and k_B is the Boltzmann constant. Using the notation ρ_n and ρ_e for the charge density of nuclei (including bound electrons) and free electrons, respectively, the electrostatic potential becomes

$$\Delta\phi(x,y,z) = -\{\rho_n(x,y,z) + \rho_{e0} \exp[e\phi(x,y,z)/k_B T]\}/\varepsilon_0. \tag{3}$$

Upon ionization, ρ_n will decrease and the density of free electrons, ρ_{e0}, will increase. This is the relation that will be used for describing the screening by the classical free electron gas. This nonlinear Poisson equation is described in some detail by Hockney and Eastwood [17] and has been used in plasma physics [18]. In our model, it is implemented into GROMACS [6], a standard molecular dynamics code, in combination with the PME algorithm [12], to simulate a Coulomb explosion. Each time step of the simulation is handled in two parts: first the Poisson-Boltzmann equation is solved while keeping the nuclei fixed, and second the positions of the nuclei are updated using molecular dynamics. The number of free electrons and their average thermal energy are also calculated during each time step. Within the approximation of a Maxwellian velocity distribution, the effective electron temperature is calculated as

$$T_e k_B = \frac{2}{3N} \sum_{i=1}^{N} E_i, \tag{4}$$

where E_i is the energy of each free electron in the sample.

III. IMPLEMENTATION

In the beginning of each time step of the molecular dynamics simulation, the initial electron density is homogeneously spread out on a grid covering the whole simulation box. The electron distribution ρ_e is determined by iteratively solving Eq. (3) until consistency is achieved. During each iteration the potential ϕ is calculated, and the iteration goes on until the total energy of the system converges. At this point, we assume that a correctly screened potential $\phi(x,y,z)$

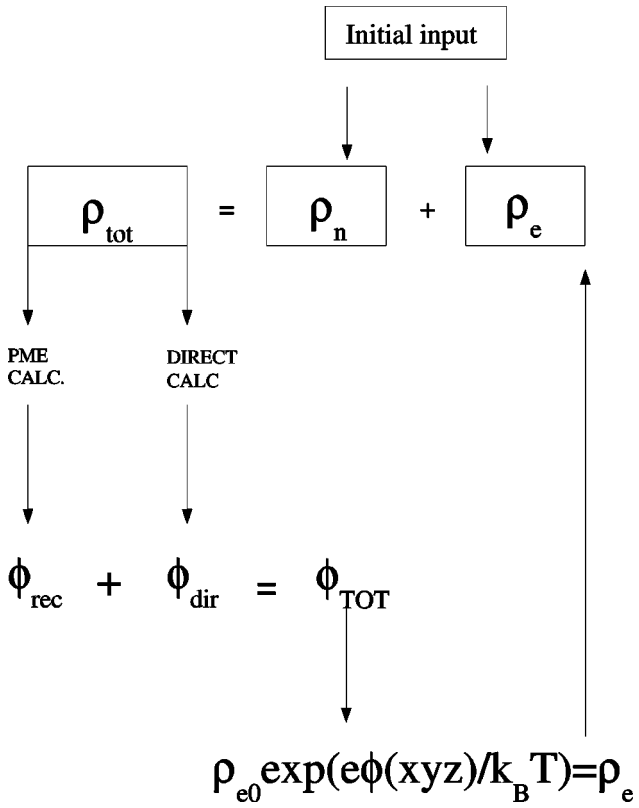

FIG. 1. Scheme of iteration for the electrostatic potential.

has been generated. In the test simulations, convergence is reached after two to five iterations. Using the principle of linear superposition for the potentials of each of the charges $q_1,\ldots,q_N$ positioned at $\mathbf{r}_1,\ldots,\mathbf{r}_N$, the electrostatic potential on the charge i due to all other charges j and all periodic images of the cell can be written as [19]

$$\phi_i = \sum_{j=1}^{N} \sum_{\mathbf{n}} \frac{q_j}{|\mathbf{r}_j - \mathbf{r}_i + \mathbf{n}|}, \tag{5}$$

where $j \neq i$ if $\mathbf{n}=(0,0,0)$. The periodic boundary condition is accounted for by the sum over the translation vectors $\mathbf{n}$, $\mathbf{n}=n_1\mathbf{a_1}+n_2\mathbf{a_2}+n_3\mathbf{a_3}$, with n_1, n_2, n_3 integers and $\mathbf{a_1}$, $\mathbf{a_2}$, $\mathbf{a_3}$ box vectors; $\mathbf{n}=(0,0,0)$ indicates the simulated cell, and all other cells are periodic images of that cell.

As the sum in Eq. (5) has to be calculated at each iteration and the system will consist of a large number of particles, the particle mesh Ewald algorithm [12] is used to speed up the calculation. The grid is transformed to reciprocal space using three-dimensional (3D) fast Fourier transformation. By splitting the sum into direct space (short-range interactions) and reciprocal space (long-range interactions), using the error function and a cutoff of 0.6 nm for the short-range interactions, convergence of Eq. (5) can be reached relatively fast. Using larger cutoffs, up to 0.9 nm, did not change our results significantly, while being computationally costly, due to the direct space calculation. The iteration process is schematically described in Fig. 1. The PME method uses periodic boundary conditions, which might seem unsuitable as the goal is to simulate the dynamics of a single sample in an x-ray beam. To overcome this problem, the simulation box has to be larger than the actual sample. Advantages of using the PME method with a large simulation box are the following.

(i) The computational cost is reduced from an order N^2 algorithm (direct sum or standard Ewald sum) to $N\ln(N)$, where N is number of grid points. Even though the simulation box has to be several times larger, the computation is considerably faster. In our case we use a grid spacing of 0.1 nm in box sizes of 6 and 12 nm, which gives $N=60^3$ and $N=120^3$, respectively.

(ii) The expansion of the exploding sample can be followed in a large box, which can be an advantage for exploding outer layers (possibly of solvent) but with a rigid sample core.

(iii) Free electrons can be allowed to leave the sample without disturbing the neutrality of the system, which is a prerequisite for the convergence of Eq. (3).

IV. RESULTS

As a test and example of the method, we present a simulation of water clusters of different sizes in vacuum. We used the simple point charge (SPC) model for the water molecules [20] and a Morse potential for the description of the chemical bonds [11]. The clusters are simulated in a Gaussian-shaped x-ray pulse with intensity 10^{12} photons/pulse and a focal spot diameter of 100 nm. The simulation was repeated with different random seeds for the stochastic processes—ionization and initial velocity of the molecules—and the results were found to be reproducible.

To illustrate the evolution of the electron gas, the electron density is plotted in the plane through the center of a small (100 molecules) cluster in a Gaussian pulse with $\sigma=10$ femtoseconds [full width at half maximum (FWHM)=23.5 fs]. This is shown at three different times in the upper part of Fig. 2. At $t=-10$ fs, the number of free electrons in the sample is starting to accumulate (a); at $t=0$ fs (at the pulse peak), the radius of gyration starts to increase, but the cluster size is still close to the original diameter of 2 nm (b). At $t=15$ fs, the radius of gyration has increased by 40%, and ions can be identified near the box boundary (c). The lower part of Fig. 2 displays snapshots of the atomic structures corresponding to the isometric plots in the upper part.

To test the stability of the model and estimate the effect of the electron screening, the Coulomb explosion of two different larger water clusters—660 molecules and 1320 molecules, respectively—has been studied in more detail. Figures 3(a) and 3(b) show the evolution of potential and kinetic energy, with and without the electron screening, for the two clusters in a Gaussian pulse with $\sigma=6$ femtoseconds (FWHM=14.1 fs). When the screening is turned off, the ionization rate is the same, but the free electrons—including the secondary electrons—do not contribute to the potential. Thus, the positive charges in the clusters are still the same in both cases, given by photoionizations, Auger decays, and ionizations through inelastic scattering, while the free electrons contribute only in the case with screening. The difference in potential energy becomes significant after the pulse

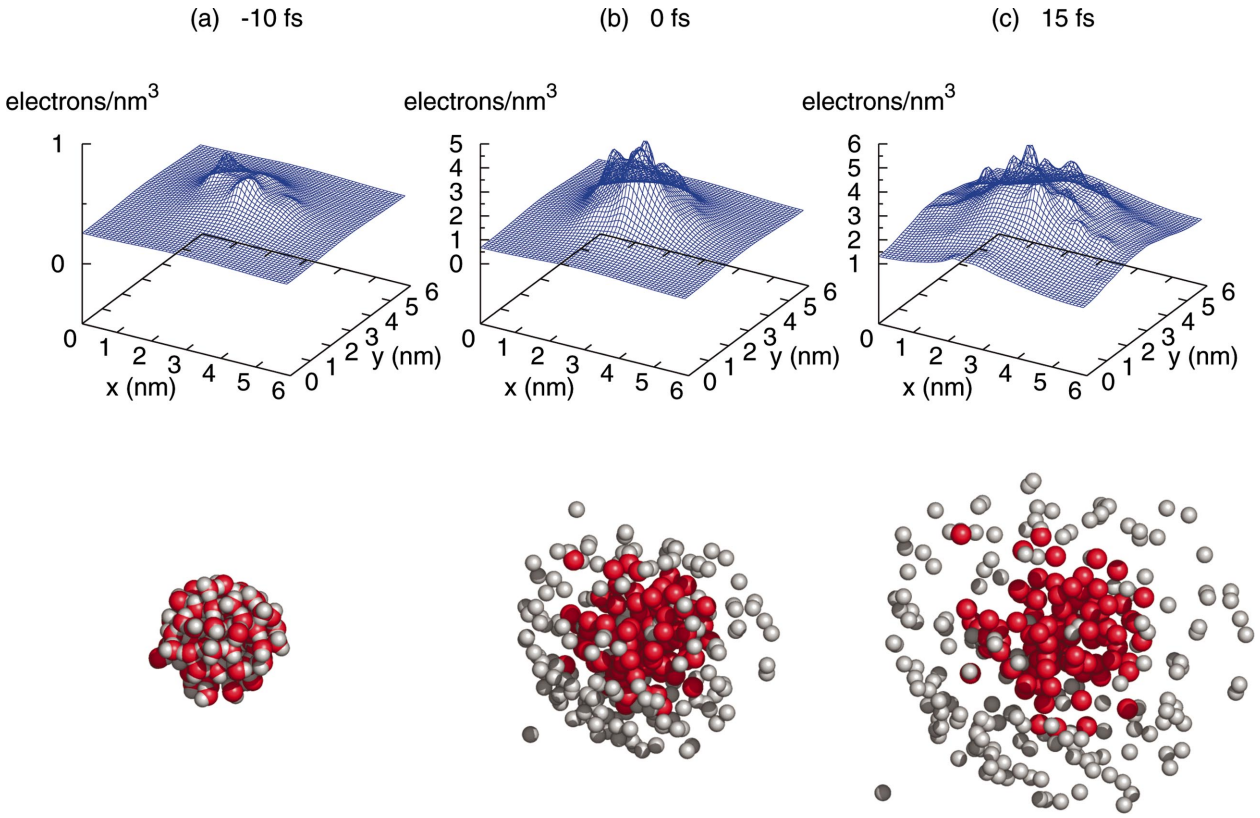

FIG. 2. (Color) Top: isometric plot of the electron distribution at (a) the beginning of the pulse (−10 fs), (b) the peak of the pulse, and (c) the end of the pulse (15 fs) for a water cluster of 100 molecules. Bottom: snapshots of the atomic structure at −10, 0, and 15 fs. Red: oxygen. White: hydrogen.

has reached its peak (time $t=0$). This is mainly due to the *K*-hole lifetime for oxygen of 6.6 fs [21]. The electron screening influences the rise of the kinetic energy of the cluster, hinting at a slowdown for the Coulomb explosion of the cluster.

The radius of gyration is used as a measure for the compactness of the structure:

$$R_g = \sqrt{\frac{\sum_i |\mathbf{r}_i|^2 m_i}{\sum_i m_i}}, \tag{6}$$

where $\mathbf{r}_i$ is the position of atom i with respect to the center of mass of the cluster and m_i is the mass of the atom. The delay in the number of accumulated electrons in the sample due to the *K*-hole lifetime also explains the small change in radius of gyration just after time zero, shown in Fig. 4. At $t=10$ fs, 95% of the x-ray pulse is over. At this time, the change in radius of gyration for the larger cluster is 13% without the electron screening. This corresponds to an expansion of the atomic structure of 2.2 Å, with a standard deviation of 0.1 Å, determined from averaging over six independent simulations, with slightly different starting conditions. With the electron screening turned on, the change in radius of gyration is damped to 10%. By analyzing the oxygen atoms separately, the radius of gyration with electron screening becomes as low as 2% [Fig. 4(b)], which corresponds to an average expansion of 0.3 Å. This indicates that

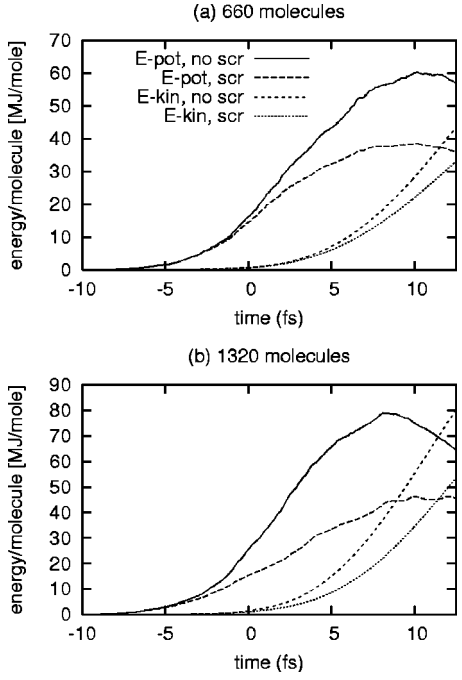

FIG. 3. Evolution of potential (E-pot) and kinetic (E-kin) energy for the atoms and ions for the two different cluster sizes, with and without electron screening. The pulse has a FWHM of 14.1 fs and an intensity of 10^{12} photons/pulse/100 nm, with the peak at time $t=0$ fs.

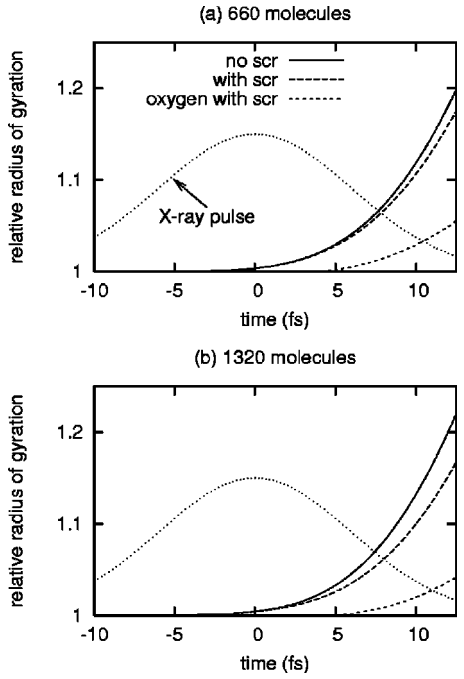

FIG. 4. Evolution of the change in radius of gyration for the two different cluster sizes of water molecules, with and without electron screening. The figure also shows the change in radius of gyration for the oxygen atoms separately, with screening.

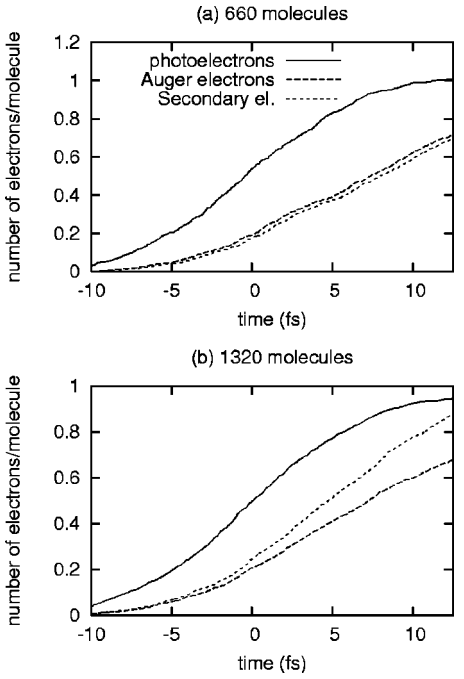

FIG. 5. Time evolution of the integrated number of electrons per molecule for the two cluster sizes: photoelectrons, Auger electrons, and their secondary electrons produced through inelastic scattering. The pulse has a FWHM of 14.1 fs and an intensity of 10^{12} photons/pulse/100 nm, with the peak at time $t=0$ fs.

the increase in radius of gyration is mainly due to the movement of the lighter dissociated hydrogen ions, while the structure of the oxygen atoms and ions is almost intact. Since elastic scattering comes mainly from inner-shell electrons of nonhydrogen atoms, this is a promising result.

The effect of the screening on the explosion dynamics is size dependent, which is expected, as more secondary electrons will be generated in the larger cluster before an Auger electron escapes. Based on our earlier calculations [13] we have estimated that an average of 1 secondary electron per Auger is produced in the 660 molecules sample versus 1.33 secondary electrons per Auger in the 1320 molecules sample. In the simulations these electrons are generated stochastically with a typical delay time constant of 0.2 fs [13]. Figure 5 shows the time evolution of the number of electrons generated inside the test samples: photoelectrons, Auger electrons, and their secondaries. While the Auger electrons are inside the sample, they contribute directly to the screening and give rise to further ionizations as described above. Due to periodic boundary conditions, the total charge in the box remains zero; thus, the Auger electrons are not removed from the simulation box after they escape the sample (the photoelectrons do not escape either; however, they are evenly spread out on the grid and do not give rise to an electric field that influences the motion of the atoms). The increasing number of the screening charges gives an indication of the importance of the screening effect and the dependence on the sample size. At $t=10$ fs, the reduction of the radius of gyration is 11% and 27% for the 660-molecule cluster and 1320-molecule cluster, respectively, thus clearly showing a dampening effect. For even larger samples more Auger and secondary electrons will be trapped, and if the potential is high enough, even photoelectrons might be trapped in the sample [10,9].

We have also looked at the radial ionic and electronic charge, averaged over solid angle, as a function of time. Figure 6 (top) shows a similar pattern for both clusters; the ionic charge density increases as the clusters are ionized and still remain close to their initial structure. As the hydrogens dissociate and expand, the charge density decreases slightly. The shell of exploding hydrogens can be seen to move faster in the larger cluster. Although the charge density of the hydrogen shell appears low compared to the cluster core in the plot, the integrated charge in a shell farther out will be large and hence give a large contribution to the electrostatic potential. This can be seen in Fig. 6 (bottom). As the electron distribution follows the potential, it will increase in the center of the cluster in the early stage of the exposure. When the Coulomb explosion starts, the electron density expands radially and decreases. For the larger cluster, it can be noted that the potential has its radial maximum somewhere in between the oxygen core and the hydrogen shell, where, apparently, the electrostatic potential is highest.

V. DISCUSSION

In this paper we have presented a computational method for including the effect of mobile electrons in a large molecule or cluster exposed to a high-brilliance x-ray source. The free electrons are modeled as a thermalized electron gas, following Maxwell-Boltzmann statistics. Including the electron gas on the simulation grid means that the interactions

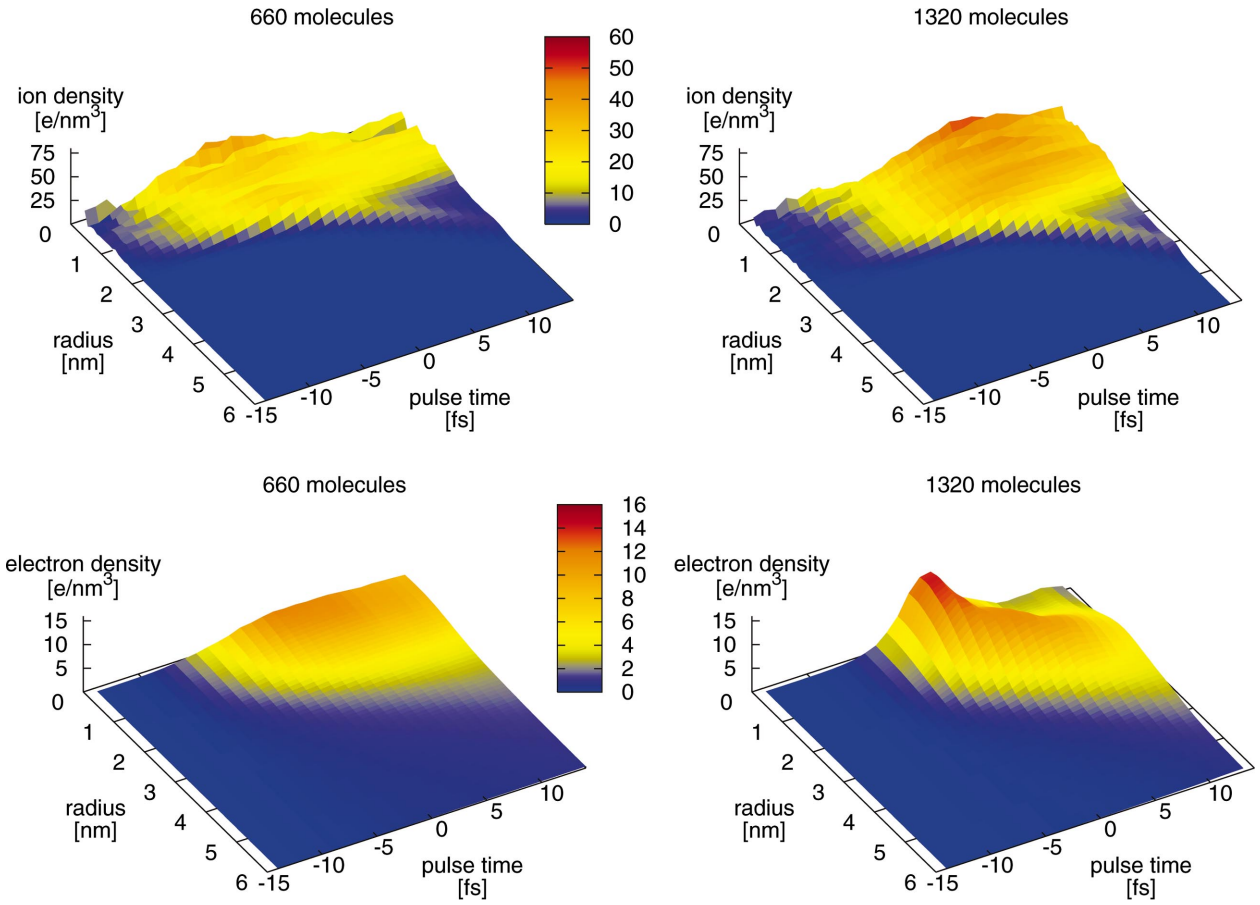

FIG. 6. (Color) Top: averaged radial ionic charge density from the center of each cluster of water molecules as a function of time. As the clusters are ionized, the ionic charge density accumulates at first and then decreases as the cluster expands. The ionic expansion is mostly due to hydrogen atoms, which can be seen as a shell propagating ahead of the oxygen ions. The hydrogen atoms are ejected a bit later in the larger cluster, but more violently. Bottom: averaged radial electron charge density from the center of each cluster of water molecules as a function of time. In the smaller cluster the electron density rises to a maximum at $t=0$ after which it decreases slightly as the atoms expand radially. In the larger cluster the electrostatic potential becomes higher, and the hydrogen atoms are pushed out more violently, followed by a spherical wave of electrons.

between all pairwise grid points have to be calculated. This can be achieved using the PME algorithm, without neglecting any of the interactions. In two recent papers different treatments of the same problem have been presented. Hau-Riege *et al.* use a one-dimensional hydrodynamics model [9], describing the electrons in a similar manner as we do. In their model, no distinction is made between the different components of the sample, although it could in principle be added. Nevertheless, this simple model catches most of the features of the model of Neutze *et al.* [5] and our current model, while it is applicable to very large samples too. On the other end of the spectrum, Jurek *et al.* have described the dynamics of a cluster of carbon atoms plus all the electrons in a classical model [10,14]. This model is probably more costly computationally than ours, although it in principle gives more detail. Both models have shown that even fast electrons can be caught in large samples and/or samples with very high ionization states. The current model is an intermediate model, based on the assumption that the plasma approximation holds. In modeling the electrons as a gas, we do not have any information about their individual dynamics, as in Ref. [10]; however, we capture the essence of their interactions, similar to the hydrodynamic model [9]. In contrast to the latter model, our model has the avantage of following the dynamics of different atomic species in a sample and of the straightforward treatment of anisotropic samples.

Our simulations of water clusters show how the Coulomb explosion slows down due to the effect of the free electrons. This dampening effect is stronger for larger clusters, which can be seen from the change in radius of gyration. At the end of the pulse, this is lowered by 11% and 39% for the 660-molecule cluster and the 1320-molecule cluster, respectively. It is also noteworthy that the oxygen atoms undergo a lower change in radius of gyration, something that was not described in the hydrodynamic model [9]. The fact that heavier atoms in a sample have a much slower increasing radius of gyration is significant and it is likely to be reflected in the diffraction patterns of the sample, where the hydrogens are not expected to contribute.

We find that the number of generated secondary electrons is an important factor which influence the explosion dynamics. If these factors can be estimated for a typical biological sample (for example using the method described in Ref. [13]), then the dynamics of such a sample can be simulated

using our algorithms for including the effect of the free electrons. Thus, extended simulations of biological samples of different composition and size can be used to optimize the pulse parameters needed for single-particle diffraction experiments.

ACKNOWLEDGMENTS

We thank Janos Hajdu, Abraham Szöke, Gyula Faigel, and Carl Caleman for illuminating discussions. This work was sponsored by the Swedish Research Council.

[1] B. H. Wiik, Nucl. Instrum. Methods Phys. Res. B **398**, 1 (1997).
[2] H. Winick, J. Electron Spectrosc. Relat. Phenom. **75**, 1 (1995).
[3] H. Wabnitz *et al.*, Nature (London) **420**, 482 (2002).
[4] J. Hajdu, R. Neutze, R. Wouts, and D. van der Spoel, in *Atomic Physics 16*, edited by William E. Baylis and Gordon W. F. Drake, AIP Conf. Proc. No. 477 (AIP, Woodbury, NY, 1999), pp. 377–385.
[5] R. Neutze, R. Wouts, D. van der Spoel, E. Weckert, and J. Hajdu, Nature (London) **406**, 752 (2000).
[6] E. Lindahl, B. A. Hess, and D. van der Spoel, J. Mol. Model. [Electronic Publication] **7**, 306 (2001).
[7] W. J. Veigele, At. Data **5**, 51 (1973).
[8] C. D. Wagner, D. A. Zatko, and R. H. Raymond, Anal. Chem. **52**, 1445 (1980).
[9] S. P. Hau-Riege, R. A. London, and A. Szöke, Phys. Rev. E **69**, 051906 (2004).
[10] Z. Jurek, G. Faigel, and M. Tegze, Eur. Phys. J. D **29**, 217 (2004).
[11] P. M. Morse, Phys. Rev. **34**, 57 (1929).
[12] U. Essman, L. Perera, M. L. Berkowitz, T. Darden, H. Lee, and L. G. Pedersen, J. Chem. Phys. **103**, 8577 (1995).
[13] N. Timneanu, C. Caleman, J. Hajdu, and D. van der Spoel, Chem. Phys. **299**, 277 (2004).
[14] G. O. Z. Jurek and G. Faigel, Europhys. Lett. **65**, 491 (2004).
[15] B. Ziaja, D. van der Spoel, A. Szöke, and J. Hajdu, Phys. Rev. B **64**, 214104 (2001).
[16] B. Ziaja, A. Szöke, D. van der Spoel, and J. Hajdu, Phys. Rev. B **66**, 024116 (2002).
[17] R. W. Hockney and J. W. Eastwood, *Computer Simulation Using Particles* (McGraw-Hill, New York, 1981).
[18] K. L. Cartwright, J. P. Verboncoeur, and C. K. Birdsall, Phys. Plasmas **7**, 3252 (2000).
[19] P. P. Ewald, Ann. Phys. (Leipzig) **64**, 253 (1921).
[20] H. J. C. Berendsen, J. P. M. Postma, W. F. van Gunsteren, and J. Hermans, in *Intermolecular Forces*, edited by B. Pullman (Reidel, Dordrecht, 1981), pp. 331–342.
[21] M. O. Krause and J. H. Oliver, J. Phys. Chem. Ref. Data **8**, 329 (1979).